



Biofilm inhibition in *Candida albicans* with biogenic hierarchical zinc-oxide nanoparticles



Kanchan M. Joshi ^{a,1}, Amruta Shelar ^{b,1}, Umesh Kasabe ^c, Latesh K. Nikam ^c, Ramdas A. Pawar ^a, Jaiprakash Sangshetti ^d, Bharat B. Kale ^e, Ajay Vikram Singh ^{f,*}, Rajendra Patil ^{g,*}, Manohar G. Chaskar ^{a,*}

^a Prof. Ramkrishna More Art, Commerce and Science College, Akurdi, Pune 411044, India

^b Department of Technology, Savitribai Phule Pune University, Pune 411007, India

^c Department of Chemistry, Baburaoji Gholap College, Sangvi, Pune 411027, India

^d Y. B. Chavan College of Pharmacy, Dr. Rafiq Zakaria Campus, Rauza Bagh, Aurangabad 431001, India

^e Nanocrystalline Laboratory, Centre for Material for Electronic Technology (CMET) Department of Information Technology, Govt. of India, Panchawati, off Pashan Road, Pune 411007, India

^f Department of Chemical and Product Safety, German Federal Institute for Risk Assessment (BfR), 10589 Berlin, Germany

^g Department of Biotechnology, Savitribai Phule Pune University, Pune 411007, India

ARTICLE INFO

Keywords:

Hierarchical ZnO NPs

Anti-virulence

Candida

Morphogenesis

Biofilm

RT-PCR

Biocompatibility

ABSTRACT

The present study demonstrates lignin (L), fragments of lignin (FL), and oxidized fragmented lignin (OFL) as templates for the synthesis of zinc oxide nanoparticles (ZnO NPs) viz., lignin-ZnO (L-ZnO), hierarchical FL-ZnO, and OFL-ZnO NPs. The X-ray diffraction patterns confirmed the formation of phase pure ZnO NPs with a hexagonal wurtzite structure. Electron microscopy confirmed the hierarchical structures with one-dimensional arrays of ZnO NPs with an average particle diameter of 40 nm. The as-synthesized L-ZnO, FL-ZnO, and OFL-ZnO NPs were tested in-vitro for growth and virulence inhibition (morphogenesis and biofilm) in *Candida albicans*. L-ZnO, FL-ZnO, and OFL-ZnO NPs all inhibited growth and virulence. Growth and virulence inhibitions were highest (more than 90%, respectively at 125, 31.2, and 62.5 µg/mL) in presence of FL-ZnO NPs, indicating that the hierarchical FL-ZnO NPs were potent growth and virulence inhibiting agent than non-hierarchical ZnO NPs. Furthermore, the real-time polymerase chain (RT-PCR) was used to study the virulence inhibition molecular mechanisms of L-ZnO, FL-ZnO, and OFL-ZnO NPs. RT-PCR results showed that the downregulation of *phr1*, *phr2*, *efg1*, *hwp1*, *ras1*, *als3* and *als4*, and the upregulation of *bcy1*, *nrg1*, and *tup1* genes inhibited the virulence in *C. albicans*. Lastly, we also performed in-vitro test cell cytotoxicity on the cell line, mouse embryo 3T3L1, and in-vivo toxicity on Rats, which showed that FL-ZnO NPs were biocompatible and nontoxic.

1. Introduction

Candida albicans is a harmless commensal organism asymptotically colonizing several niches in the body, including but not limited to the gastrointestinal (GI) tract, female reproductive tract, oral cavity, and skin [1–3]. However, under an altered immune system, or variation in the local environment such as pH, and antibiotics abuse or alteration in the nutritional status, *C. albicans* turns into an opportunistic pathogen, causing localized or systemic infections [4]. *C. albicans* shows physical plasticity called morphogenesis, in which the morphology of *C. albicans* switches from yeast form to hyphal form. As a result of morphogenesis, *C. albicans*

can more easily penetrate mucous membranes, invade tissues, and enter the bloodstream, which increases the risk of tissue damage [5]. Morphogenesis also helps *C. albicans* to escape the phagocytosis of macrophages [6,7]. *C. albicans* also exhibit virulence through their ability to form biofilms on abiotic or biotic surfaces. Biofilms are communities of yeast, pseudohyphal and hyphal cells enclosed in a polymeric extracellular matrix (EPM) [8–10]. *C. albicans* are highly resistant to antimicrobial agents and host immune factors due to the complex architectures of biofilms [11–14]. The EPM in the biofilm provides structural integrity and protects cells from the surrounding environment. Thus, targeting the virulence systems - morphogenesis and biofilm - has become a promising strategy to stop the progression of *C. albicans*.

In the past, there have been attempts to design anti-virulence molecules, such as small molecules from microorganisms and plants [15,16], and nanozymes [17–19], to target the virulence system of *C. albicans*. Nanozymes such as citrate-coated Fe₃O₄ NPs were efficiently demonstrated to possess antibacterial activity over a wide range of pH by utilizing

* Corresponding authors.

E-mail addresses: Ajay-Vikram.Singh@bfr.bund.de (A.V. Singh), rpatil@unipune.ac.in (R. Patil), dean.st@unipune.ac.in (M.G. Chaskar).

¹ Both authors contributed equally.

adenosine triphosphate disodium salt (ATP) as a synergistic agent to accelerate the hydroxyl (*OH) radical production [19]. Some of the NPs mentioned above had limited success, while others have not been tested to determine whether they inhibit biofilm formation by *C. albicans*. Several studies have shown that nanomaterials (nanosized particles with altered physical and chemical properties) inhibit microbial growth in solution and surfaces [20–23]. Nanomaterials such as silver (Ag), zinc oxide (ZnO), magnesium oxide (MgO), iron oxide (Fe₃O₄), and copper (CuO and Cu₂O) have been used successfully to inhibit or kill *C. albicans* [20]. Nevertheless, only Ag, ZnO, NPs, MgO, Fe₃O₄, CuO, and selenium (Se) NPs have been reported to inhibit the virulence system of *C. albicans* [24–35]. In *C. albicans*, Ag NPs showed antibiofilm activity by inhibiting the key genes mediating yeast to hyphal transition (*ece1*, *tec*, *tup1*, and *rfg1* genes), disrupting β -glucan synthase and membrane architecture (pit and holes formation on cells), altering the membrane fluidity (altering cellular ergosterol and oleic acid compositions) and by inhibiting the production of extracellular enzymes (proteinase, phospholipase, hemolysin, and lipase) [20]. The Se NPs, which are less toxic to mammalian cells than Ag NPs, attach to the cell wall, penetrate through it, and replace sulfur with Se in important biochemical processes [36]. ZnO-NPs inhibit hyphal formation by producing ROS [23], and CuO and Cu₂O, respectively, elicit ROS and membrane damage to constrain the yeast for hyphal formation [37]. Fe₃O₄ NPs showed anti-biofilm activity by directly affecting cell viability and metabolic processes of cells [38]. While all the above nanomaterials have gained significant importance in the field of antimicrobial applications, ZnO NPs have gained particular importance due to their broad direct bandgap (3.37 eV) that is essential for providing NPs with photocatalytic properties. Additionally, ZnO NPs were found to be non-toxic and biocompatible, have been used as drug carriers, cosmetic ingredients, and filling materials in medical applications.

Lignin is a complex macromolecule of plant origin located in the secondary cell walls. Lignin is a heteropolymer containing randomly crosslinked phenylpropanoid units (coumaryl, coniferyl, and sinapyl alcohol). Phenylpropanoids are connected through several types of linkages, mainly ether bonds such as alkyl- or phenyl ether and carbon-carbon bonds such as biphenyl, diphenyl ethane, and pinoresinol. Recent studies have indicated that lignin is a valuable NPs synthesis material because it can avoid the drawbacks of chemical methods of NPs synthesis such as aggregation, re-precipitation, bulking, and stability that cause poor NP performance for biomedical applications. Lignin is biodegradable and biocompatible, which makes it an excellent precursor for developing eco-friendly nanoscale materials. Lignin interacts directly with the surface of synthesized NPs, causing them to become stable and providing a protective coating to prevent agglomeration and polydispersity of the synthesized NPs [39,40].

The present study explored lignin, FL, and OFL as templates for synthesizing ZnO NPs and studied the potential of as-synthesized L-ZnO, FL-ZnO, and OFL-ZnO NPs to inhibit growth and virulence in *C. albicans*. The molecular mechanism of action of FL-ZnO NPs was further explored by examining the gene expression profiles involved in virulence. The present study attempts to use agriculture waste, lignin, as a bio template to synthesize anti-*Candida* and anti-virulence NPs against *C. albicans*.

2. Experimental sections

2.1. Chemicals used in the study

For the present study, all chemicals were purchased from Loba Chemicals, Mumbai, culture media from Hi-Media, Mumbai, RNA extraction kit from Qiagen, USA, cDNA synthesis kit, and RT-PCR master mix from Applied Biosystems, USA. Sugarcane bagasse was obtained from a local mill and washed twice with 0.1 N hydrogen chloride (HCl) and distilled water to remove dust particles and acid-soluble cellulose. The material was dried in the air and crashed into 100 mesh particles. The ATCC 227 strain of *Candida albicans* was a kind gift from Dr. Zore, SRTMU, Nanded.

2.2. Microwave-assisted extraction of lignin from bagasse

A Samsung microwave oven (700 W, India) was used to isolate lignin from bagasse. Twenty grams of bagasse particles were soaked in 200 mL of 0.1 N HCl for 24 h and filtered. The retentates were washed several times with water and then treated with 100 mL of hydrogen peroxide (H₂O₂) containing 3 g of sodium hydroxide (NaOH). Afterward, the mixture was microwaved for 30 min at 400 W and filtered. The filtrate was acidified with sulfuric acid to a pH of 2 to 3 and then precipitated with ethanol and ether [41].

2.3. Fragmentation of lignin

An air-dried, purified 5 g of lignin was dissolved in 50 mL of 0.1 M NaOH solution at pH 12 and stirred for 30 min at 40–50 °C. After that, 100 mL of 30% (%) H₂O₂ solution was added dropwise to the solution for 1 h. The resultant solution was cooled and acidified with H₂SO₄ (pH 4 to 5), resulting in the formation of the ivory-colored precipitate. Further purification occurred using column chromatography (15-cm column height, stationary phase silica gel 60–120 mesh, mobile phase 30% ethyl acetate, and 70% n-hexane) [41].

2.4. Oxidation of fragmented lignin (FL)

A 0.5 g FL was added into 100 mL of 0.1 N NaOH solution and stirred for 30 min, and then 0.5 g of potassium permanganate was added slowly, and the mixture stirred at 40 °C for 3 h, and later kept at 27 °C for 15 to 20 h. The product was filtered off and precipitated by using dilute HCl solution. The product was recrystallised in hot water by washing with cold water [41].

2.5. Synthesis of zinc oxide nanoparticles (ZnO NPs)

The direct co-precipitation method was used for the synthesis of ZnO NPs. About 0.1 g of each lignin, FL, and OFL were added separately in 0.1 M 100 mL solution of NaOH and then sonicated for 1 h to get the homogenous solution. After sonication, 2 g of zinc acetate was added, heated at 90 °C, and stirred for 1 h to get precipitation. The precipitate was a wash with distilled water and alcohol, followed by drying at 90 °C [47].

2.6. Characterization of ZnO NPs

The fragmentation pattern of lignin was studied using nuclear magnetic resonance spectroscopy (NMR, Bruker Avancell 500 MHz Spectrometer) and high-resolution mass spectrometer (HRMS, Impact-II UHR-TOF Mass Spectrometer System, 100 to 3500 *m/z*). The synthesis of ZnO NPs was followed by UV-visible spectroscopy (UV-Vis, Shimadzu-DRS-2600) and X-ray diffraction (XRD, Advance Bruker D8). The morphology of ZnO NPs was observed by using field emission scanning electronic microscopy (FESEM, Hitachi S-4800 Tokyo, Japan) and transmission electron microscopy (TEM, Jeol, Jem-2200FS). The surface area of NPs was determined using Brunauer–Emmett–Teller (BET) on Micromeritics 2720 (Chemisoft TPX).

2.7. Effect of L-ZnO, FL-ZnO and OFL-ZnO NPs on the planktonic growth of *C. albicans*

Standard broth microdilution method based on the guidelines of Clinical Laboratory Standards Institute [42] was used to study the effect of lignin, FL, and OFL and L-ZnO, FL-ZnO, and OFL-ZnO NPs on the planktonic growth of *C. albicans*. 100 μ L solution containing various concentrations of above samples ranging from concentration of 3.9 to 500 μ g/mL were prepared in Roswell Park Memorial Institute (RPMI)-1640 medium, and cells of *C. albicans* (1×10^3 cells/mL) were added into 96 well plates (Costar, Corning Inc. USA). The plates were incubated at 37 °C for 24 h, and growth was measured by recording the optical absorbance at 620 nm using a microplate reader (Hidex, Germany). The minimum concentrations of L-ZnO, FL-

ZnO, and OFL-ZnO NPs that reduce the growth of a planktonic form of *C. albicans* by more than 90% were considered as the minimum inhibitory concentrations (MIC). Similarly, the concentration of compounds that caused a 50% reduction in the growth was considered MIC₅₀. Control samples have proceeded in similar conditions without lignin, FL, OFL and L-ZnO, FL-ZnO, and OFL-ZnO NPs. Experiments were done in triplicates ($n = 3$). Data are reported as mean \pm standard deviation.

2.8. Determination of reactive oxygen species (ROS)

The ROS generations in *C. albicans* cells (1×10^6 cells/mL) were measured by subjecting cells to FL-ZnO NPs (31.25 $\mu\text{g/mL}$) for 30 min. After the treatment, cells were resuspended in 1 mL phosphate-buffered saline (PBS) containing 5 μL of 2',7'-Dichlorofluorescein diacetate (10 μM) and incubated at 37 °C for 15 to 30 min. After incubation, cells were washed, centrifuged at 1400 g, and resuspended in 500 μL PBS by gently flicking the tubes. The fluorescent cells were analyzed with Attune NxT Glow Flowcytometer (Thermo Fisher Scientific, USA). Gate was on the cells, excluding debris. Cells treated H₂O₂ (10 $\mu\text{g/mL}$) were used as a positive control.

2.9. Morphogenesis inhibition assay

Morphogenesis inhibition was studied in a 20% bovine serum medium (BSA) [43]. In this test, various concentrations (ranging from 3.9 to 500 $\mu\text{g/mL}$) of lignin, FL, and OFL and L-ZnO, FL-ZnO, and OFL-ZnO NPs were each subjected separately to 1×10^5 cells/mL in 20 mL BSA medium and incubated at 37 °C for 90 min. After incubation, morphogenesis (induction of germ tube) was observed microscopically (Leica, Japan) using fluorescent dye Con-A Alexa 488 (excitation and emission wavelength, respectively, 480 and 520 nm). Control samples have proceeded in similar conditions without lignin, FL, OFL and L-ZnO, FL-ZnO, and OFL-ZnO NPs. Experiments were done in triplicates ($n = 3$).

2.10. Biofilm inhibition assay

Biofilm inhibition assay was performed in 96-well polystyrene tissue culture-treated plates [44]. 100 μL volume of cell suspensions (1×10^7 cells/mL) were seeded in each well and allowed to adhere to the surface of polystyrene tissue culture at 37 °C for 90 min. After adhesion, cells were repeatedly washed with phosphate-buffered saline (PBS), pH 7 and 0.1 M various concentrations of lignin, FL, and OFL and L-ZnO, FL-ZnO, and OFL-ZnO NPs ranging from 3.9 to 500 $\mu\text{g/mL}$ were prepared in RPMI-1640 medium. 200 μL of these concentrations were added to the previously seeded 96 well plates and incubated for 24 h at 37 °C. After 24 h, the non-adhered cells were removed and aseptically washed biofilm to remove unadhered cells and subjected to 50 μL of 2 mg/mL solution of 3-(4,5-dimethylthiazol-2-yl)-2,5-diphenyltetrazolium bromide, a tetrazole (MTT) for 3 h under dark conditions. After 3 h, 100 μL of dimethyl sulfoxide was added to each well, and optical absorption was read at 580 nm using a microplate reader (Hidex, Germany). All experiments were done in triplicates. The minimum concentrations of L-ZnO, FL-ZnO, and OFL-ZnO NPs that inhibited the biofilm of *C. albicans* by more than 90% were considered as the minimum inhibitory concentrations (MIC). Similarly, the concentration of compounds that caused a 50% biofilm inhibition was considered as MIC₅₀. The morphological features of biofilm at MIC₅₀ value in the presence of L-ZnO, FL-ZnO, and OFL-ZnO NPs were observed by fluorescent staining. After biofilm was washed with PBS, 25 μL of 1 $\mu\text{g/mL}$ of Con-A Alexa was added to each well, and incubated for 30 min, washed repeatedly, and observed under a confocal microscope (NIKON A1 R) with excitation and emission wavelength, respectively at 480 and 520 nm. Control samples have proceeded in similar conditions but without lignin, FL, OFL. Experiments were done in triplicates ($n = 3$). Data are reported as mean \pm standard deviation.

2.11. Gene expression analysis

The gene expression analysis during morphogenesis in the presence of L-ZnO, FL-ZnO, and OFL-ZnO NPs was measured using real-time polymerase chain reaction (RT-PCR) [44]. In short, 1×10^6 cells/mL were inoculated separately into 20% BSA medium, each containing MIC₅₀ concentrations of L-ZnO, FL-ZnO, and OFL-ZnO NPs, and incubated for 90 min at 37 °C at 150 rpm. Cells were lysed with lysis enzyme, and the RNA was isolated using RNeasy® Mini Kit (QIAGEN, USA) as per manufacture protocol. Further, the total RNA was converted to cDNA using SuperScript®III (Invitrogen, Life Technologies, USA) as per manufacture instructions. The RT-PCR was performed on (CFX 96 Real-time System, Bio-Rad, USA) by using KAPA SYBR® Fast qPCR Kit Master mix (2 \times) (BIOSYSTEMS, South Africa). The primers used in the study were mentioned in Table 1. The gene expression levels were calculated using the formula $2^{-\Delta\Delta C}$. All the experiments were done in triplicates ($n = 3$). Data are reported as mean \pm standard deviation.

2.12. In-vitro cell cytotoxicity study

Toxicity study of FL-ZnO NPs was performed on a 3T3L1 (fibroblast) cell line from the mouse embryo. The cell line was a kind gift from our colleague in the Department. 3T3L1 cells in Dulbecco's Modified Eagle's Medium (DMEM) containing 10% Fetal Calf Serum (FCS), 4 mm Glutamine, and 1% antibiotic/antimycotic, in a 5% CO₂ incubator at 37 °C. Briefly, 100 μL of 3T3-L1 cells were seeded into 96-well plates (1×10^3 cells/well) and treated with various concentrations of FL-ZnO NPs for 24 h. After incubation, 20 μL /well of MTT solution (50 $\mu\text{g/mL}$) was added and further incubated for 3 h at 37 °C in a humidified 5% CO₂ atmosphere. After incubation, the plate was spin at 2000 g for 5 min, and 100 μL was replaced with 100 μL DMSO, and optical density was recorded at 570 nm using a microplate reader (Hidex, Germany).

2.13. In-vivo animal study

Toxicity testing of FL-ZnO NPs was performed on rats at the Department of Veterinary Pathology, Krantisinh Nana Patil College of Veterinary Science (KNPCVS), Shirval, Dist. Satara. The animal experiments were performed per India's Committee for the Control and Supervision on Animals (CPSEA) guidelines. Prior approval was sought from the Institutional Animal Care and Use Committee of the KNPCVS. The rats were fed with 100 mg of FL-ZnO NPs for 28 days and monitored daily for weight. Rats

Table 1
Genes used to study morphogenesis and biofilm inhibition in *C. albicans*.

Primers (genes)	Sequence (5' \rightarrow 3')
ACT1N R	ACCTCTTTTGGATTGGGCTTCA
ACT1N F	ATG GACGGTGAAGAAGTTGC
PHR1 R	AAGCTGTAGTGGAGCTGCA
PHR1 F	GGTCTGCTGCTGTGATGAT
PHR2 R	TCTGCTGGCTCTTCAGGATT
PHR2 F	CCACTTGAACCAGATGACGA
EFG1 R	TTGTTGCTGCTGTCTGTCTC
EFG1 F	TATGCCCCAGCAACAACCTG
RAS1 R	GTCTTTCCATTTCATAAATCAC
RAS1 F	GGCCATGAGAGAACAATATA
NRG1 R	GCCCTGGAGATGGTCTGA
NRG1 F	CACCTCACTTGCAACCCG
TUP1 R	GGCGACGCGTCTTTTTTGGTCCATTTCCAAATTTCTG
TUP1 F	GAGGATCCCATTGATCCCCAACGCCACCCAG
HWP1 R	CAATAATAGCAGCACCAGG
HWP1 F	TGGTGCTAATTAATTTCCGG
BCY1 R	GGGCTGCAGTTAATGACCAGCAGTTGGGT
BCY1 F	CCCAGCTTATGTCTAATCTCAACAGCA
ALS3 R	CAGCAGTAGTAAACAGTAGTAGTTTCATC
ALS3 F	CCACTTCACAATCCCCATC
ALS4 R	GTAATGAGTCATCAACAGAAGCC
ALS4 F	CCCAGCTTTTCAACAGCAGTAAAT

were sacrificed with cervical dislocation, and organs were observed for histopathological studies. The respective organ specimens were fixed in phosphate buffer (pH 7.4) containing 4% formalin for histopathological studies. The tissue sections of the liver, kidney, and heart, after fixation, were processed on an automated tissue processor for the histopathological protocol using ascending grades of alcohol and cleared in xylene. The tissue was embedded in paraffin blocks for micro-sectioning on the automated tissue microtome (Leica, Germany). The tissue sections of 5 μm were taken on glass slides. The tissue sections were stained by routine hematoxylin and eosin protocol and were observed under a binocular microscope with a microphotography unit. (Nikon, Japan). The histopathological examination was performed for cellular pathological changes.

2.14. Statistics

In the present study, cell viability data were presented as mean (\pm) standard deviations (SD), which were obtained from three independent experimental repeats. One-way ANOVA followed by Dunnett's post hoc test with GraphPad Prism software (GraphPad Software, Inc., La Jolla, CA, USA) for the statistical analysis. $P < 0.05$ was considered to indicate a statistically significant difference.

3. Results

3.1. Characterization of lignin, FL, and OFL

The UV-Vis spectra of extracted lignin, FL, and OFL are shown in Fig. 1 (A). Extracted lignin showed an absorption maximum at 287 nm, and the OFL showed two peaks, one at 280 nm and the other at 317 nm. The FL showed an entirely different spectrum. The FL showed an absorption maximum at 424 nm. To further support the UV-Vis spectroscopy study, we have performed FTIR [Fig. 1(B)]. The FTIR of FL showed two broad peaks, one at 1500–1627 cm^{-1} and the other at 800 cm^{-1} to 4000, $^{-1}$ a significant peak at 3458 cm^{-1} and other small peaks at 1726 cm^{-1} , 1627 cm^{-1} , 3372 cm^{-1} , 1712 cm^{-1} , 1050 cm^{-1} and 1158 cm^{-1} . The FTIR spectrum of OFL showed significant peaks in the region between

500 cm^{-1} to 3000 cm^{-1} , and an intense peak at 1726 cm^{-1} . To identify the FL, we performed HRMS. HRMS analysis showed five fragments. The first fragment at 276 m/z , the second fragment at 290 m/z , the fourth fragment at 405 m/z , and the fifth fragment at 534 m/z [Fig. 2 (A) and (B)]. Furthermore, we also performed NMR to ascertain fragmentation of lignin and oxidation of fragmented lignin. In NMR, FL showed peaks at 0.9–1.5 δ , 3.5–4.2 δ , 4.8–5.8 δ , and 6.8–7.4 δ , OFL showed a peak at 9.8 δ .

3.2. Characterization of L-ZnO, FL-ZnO and OFL-ZnO NPs

The synthesis of ZnO NPs was followed by UV-Vis spectroscopy [Fig. 3 (A)] and XRD [Fig. 3 (B)]. In UV-Vis spectroscopy, the sharp absorption peaks for L-ZnO, FL-ZnO and OFL-ZnO NPs were observed at 368, 360, and 370 nm, respectively. There was a significant blue shift in the exciton absorption for FL-ZnO NPs, indicating the quantum confinement property of FL-ZnO NPs. A tau plot calculated bandgap values for L-ZnO, FL-ZnO and OFL-ZnO NPs, respectively, were 3.04, 3.16 and 3.18 eV. In XRD, the structure and phase of L-ZnO, FL-ZnO, and OFL-ZnO NPs were studied. Scherrer equation was used to calculate the crystallite size $\frac{kl}{\beta \cos \theta}$, where D is the mean grain size, k is the dimensional less shape constant (0.9), λ is the wavelength of the X-ray, β is the broadening at half full width half maximum, and θ is Bragg angle respectively. The major XRD peaks for L-ZnO, FL-ZnO, OFL-ZnO NPs are shown in Fig. 3 (B). The observed peak at $2\theta = 31.61^\circ, 34.32^\circ, 36.14^\circ, 47.37^\circ, 6.48^\circ, 62.71^\circ$ and 68.28° correspond to (100), (002), (101), (110), (103), (201), (112) planes. In XRD, the intensity of the (101) plane was higher than the (100) plane. The average crystallite size for L-ZnO, FL-ZnO, OFL-ZnO NPs was 40–44 nm. The morphology of L-ZnO, FL-ZnO and OFL-ZnO NPs were studied by SEM [Fig. 3(C)]. The L-ZnO NPs were spherical and agglomerated. The detailed morphological analysis of FL-ZnO NPs was performed by TEM [Fig. 3 (C)]. In TEM, nanorods with an average diameter of 30 nm were observed with interplanar spacings of 0.2798 nm [Fig. 3 (C)], corresponding to the (100) plane of ZnO. Interestingly, pores with an average diameter of 2 nm were also observed on the surfaces of FL-ZnO NPs. BET measurements further confirmed the porous structure of FL-ZnO NPs. In BET, the specific surface measurement for FL-ZnO NPs was 132 m^2/g instead of 115 m^2/g for pristine ZnO NPs.

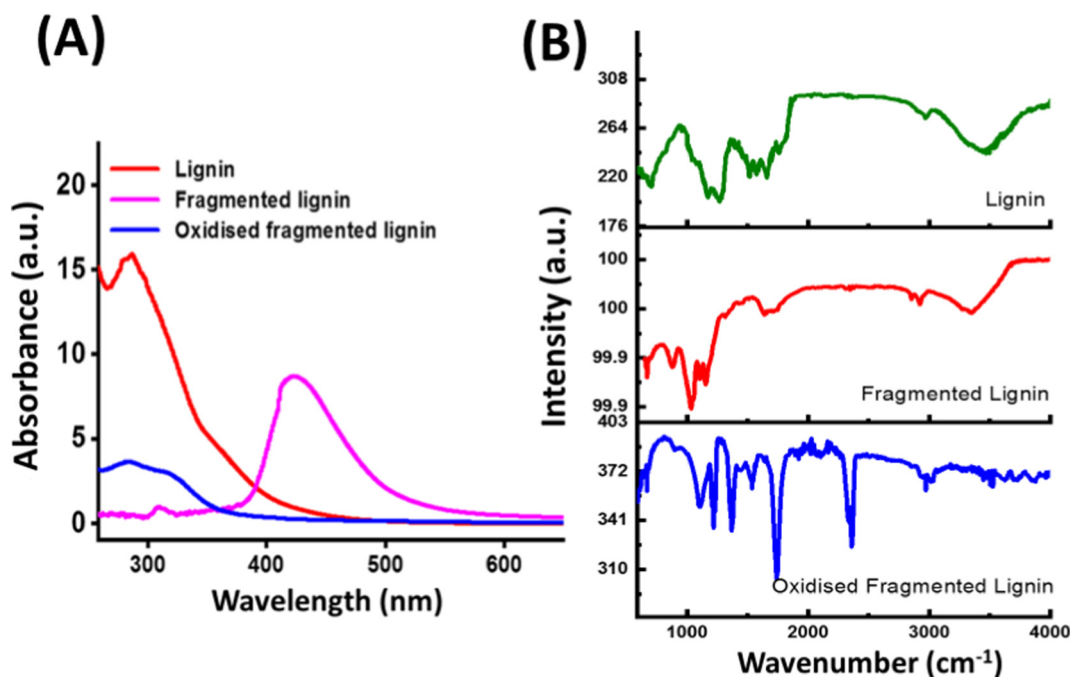


Fig. 1. (A) UV-Visible spectrum of extracted lignin, fragmented lignin, and oxidized fragmented lignin. The UV-Vis spectrum of extracted lignin and oxidized fragmented lignin matches each other (λ_{max} is around 300 nm). However, λ_{max} of fragmented lignin showed an additional peak at 415 nm. (B) FTIR analysis of lignin, fragmented lignin, and oxidized fragmented lignin (OFL). The characteristic functional group in each is visible.

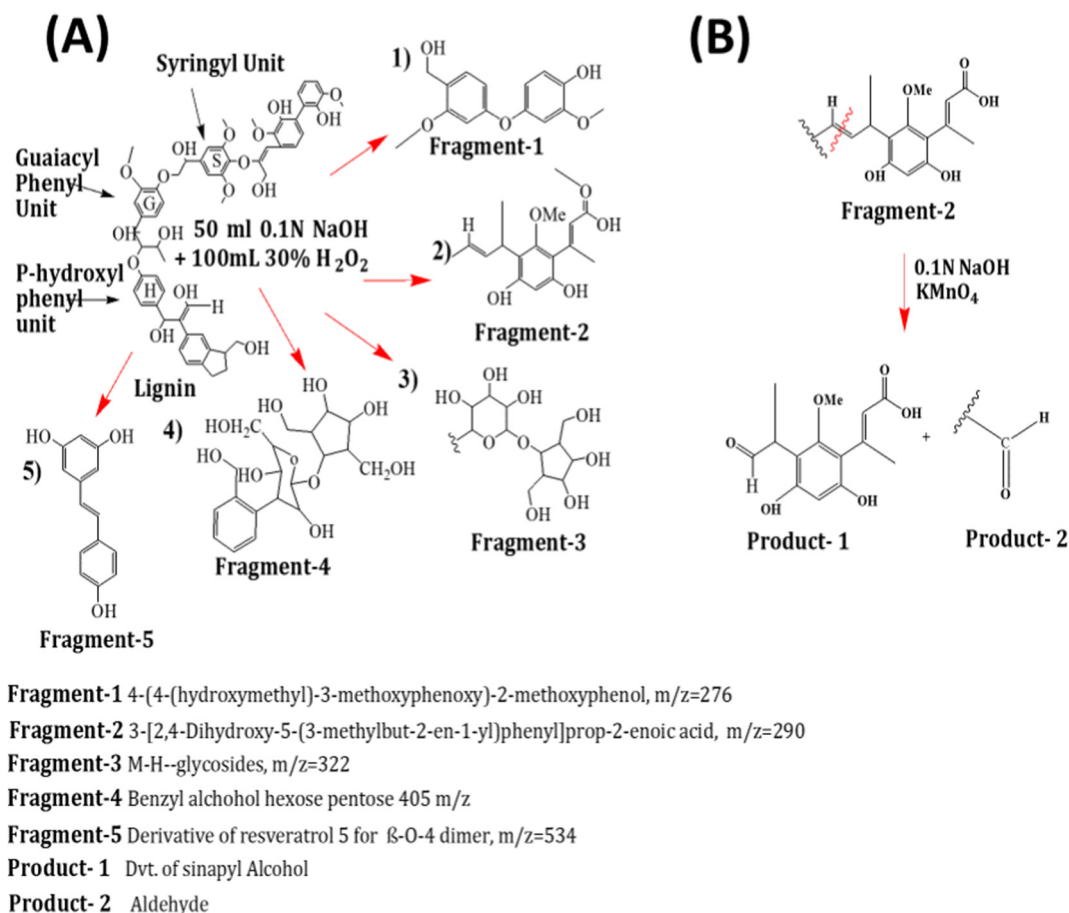


Fig. 2. (A) Fragmentation pattern of lignin and (B) oxidation pattern of fragmented lignin (OFL).

3.3. Effect of L-ZnO, FL-ZnO and OFL-ZnO NPs on the planktonic growth of *C. albicans*

The abilities of L-ZnO, FL-ZnO and OFL-ZnO NPs to inhibit the growth of *C. albicans* was assayed by determining MIC [Fig. 4(A)]. As shown in Fig. 4(A), when the cells of *C. albicans* were subjected to L-ZnO, FL-ZnO and OFL-ZnO NPs, it was observed that the % cell viability reduced, the highest reduction observed in the presence of FL-ZnO NPs followed by OFL-ZnO NPs, and lowest reduction in the % cell viability was observed in the presence of L-ZnO NPs. A 100% reduction in cell viability was observed in the presence of FL-ZnO NPs. The MIC₅₀ concentrations of L-ZnO, FL-ZnO and OFL-ZnO NPs against *C. albicans* were, respectively, 465.8, 7.31 and 31.25 μg/mL. The % cell viability reduction in the presence of lignin, FL, and OFL was between 5 and 7%. Next, we studied if ROS has some role in inhibiting the growth of *C. albicans*. A flow cytometer was used to quantify the levels of ROS in cells. As shown in Fig. 5 (B), the level of ROS generated in control cells (without treatment) was 0.650%, and levels of ROS generated in FL-ZnO were 4.87%. The level of ROS in the presence of H₂O₂ was 26.93%.

3.4. Morphogenesis inhibition

The abilities of L-ZnO, FL-ZnO and OFL-ZnO NPs to inhibit the morphogenesis in *C. albicans* was studied by observing the distinct morphological cells (oval Vs hyphal) under a fluorescent microscope. Under a fluorescent microscope [Fig. 4 (C)], the presence of L-ZnO, FL-ZnO, and OFL-ZnO NPs inhibited the morphogenesis (oval-shaped cells observed). The MIC of L-ZnO, FL-ZnO and OFL-ZnO NPs that inhibited morphogenesis respectively were 500, 31.2 and 62.5 μg/mL. It appeared that morphogenesis was

inhibited strongly in the presence of FL-ZnO NPs. Lignin, FL and OFL have not inhibited morphogenesis. The control cells (without being subjected to NPs) showed hyphal induction.

3.5. Biofilm inhibition

As shown from Fig. 4 (B), L-ZnO, FL-ZnO, and OFL-ZnO NPs inhibited biofilm to varying degrees. As expected, the % biofilm inhibition was highest in the presence of FL-ZnO NPs. More than 80% of the biofilm was inhibited in the presence of FL-ZnO NPs at 31.25 μg/mL; however, at the same concentration, L-ZnO and OFL-ZnO NPs inhibited biofilm to a lesser extent. The biofilm inhibition was slightest in the presence of L-ZnO NPs. A 50% biofilm inhibition was observed at approximately 262, 3.25, and 29.48 μg/mL, respectively, in the presence of L-ZnO, FL-ZnO, and OFL-ZnO NPs. As expected, lignin, FL and OFL did not inhibit the biofilm. Confocal microscopic observation of biofilm also has shown that biofilm inhibition was more significant in the presence of FL-ZnO NPs [Fig. 4 (B)]. In the control (at 0 μg/mL), there was a confluent biofilm. However, at 31.25 μg/mL, the confluence of biofilm decreased in the presence of L-ZnO, FL-ZnO and OFL-ZnO NPs. Moreover, the confluent growth is reduced by 30 and 50%, respectively, when L-ZnO or OFL-ZnO NPs were present, while more than 80% is reduced when FL-ZnO NPs were present.

3.6. Gene expression analysis

To understand the molecular mechanisms behind morphogenesis, we performed an RT-PCR study. We have selected a few essential genes (Table 1) which have been shown to play prominent roles in the morphogenesis and biofilm of *C. albicans*. In the present study, the negative regulators of morphogenesis and biofilm, such as *bcy1*, *nrg1*, and *tup1* were

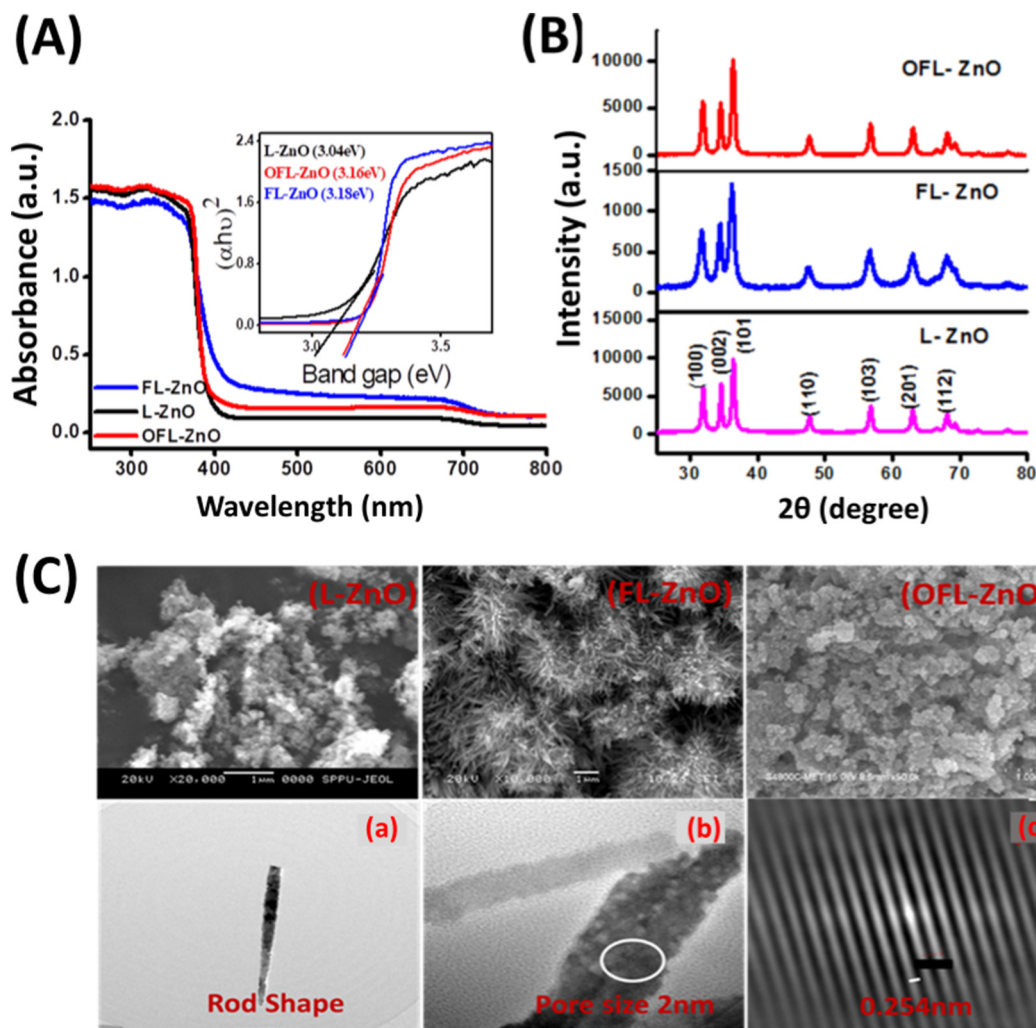


Fig. 3. (A) UV-Visible spectrum of L-ZnO, FL-ZnO, OFL-ZnO NPs. Inset: The Tauc plot of the calculated band gap of L-ZnO, FL-ZnO and OFL-ZnO NPs, (B) XRD of ZnO NPs prepared by using lignin, fragmented lignin and oxidized fragmented lignin, (C) Morphological analysis of ZnO NPs: (Upper) - In SEM, L-ZnO and OFL-ZnO NPs were aggregated mass of spherical NPs, however, FL-ZnO NPs were hierarchical flower-like structures; (Lower) - In TEM, the hierarchical unit of FL-ZnO NPs is seen as rod shaped structures with pores on it.

upregulated in a range of 2.3 to 13.3 folds. In contrast, the positive regulators of morphogenesis and biofilm such as *phr1*, *efg1*, *hwp1*, *ras1*, *als3* and *als4* were downregulated in a range of 0.004 to 0.433 folds [Fig. 5 (A)].

3.7. Biocompatibility study of FL-ZnO NPs

Biocompatibility studies of FL-ZnO NPs were performed by in-vitro cell cytotoxicity studies on 3T3-L1 cells and in-vivo toxicity studies on Rats. As shown from Fig. 6 (A), the % viability (growth) of 3T3-L1 cells at 12 $\mu\text{g}/\text{mL}$ was more than 85%, indicating the non-cytotoxic nature of FL-ZnO. In-vivo animal studies [Fig. 6 (B)] showed that when the Rats (average weight 250 g) were fed with a daily dose of 100 mg of FL-ZnO NPs and observed for health parameters for 28 days, it was observed that the average weight of Rats remained constant till 12 days, and after that increased gradually till 28 days. However, the weight of control Rats remained relatively constant, around 260 g. The reason for the increased weight of Rats when fed with FL-ZnO NPs is, at present is not clear to us.

Furthermore, histological tissue sections of the kidney, heart, and liver of FL-ZnO NPs treated Rats had no abnormalities in any tissue sections treated with [Fig. 6 (C)]. Histopathological study of liver tissues showed normal histomorphology of the hepatocytes and the vascular network. The hepatic parenchyma showed classic hepatic lobules with hepatic cords and central veins with their central axis. The portal triad showed normal

histomorphology of bile ducts, hepatic artery and portal vein. The hepatocytes were round and polygonal in shape-containing round vesicular nuclei. The hepatic sinusoids appeared normal with the occasional presence of Kupffer cells. There was an absence of any pathological or metabolic changes in the liver tissue sections examined. The histological examination of kidney tissue sections showed normal cellular details of glomeruli and renal tubules with normal vascular tissue. The cortex region showed the presence of normal histomorphology of glomeruli with Bowman's capsule and a tuft of capillaries. The proximal and distal convoluted renal tubules were intact and uniform with tubular epithelium and lumen. There was an absence of any pathological or metabolic changes in the kidney tissue sections examined. The histological examination of heart tissue sections showed normal and intact cardiac myofibers arranged in uniform length with the focal presence of vascular tissue in the pericardium layer. The cardiac muscle fibres were compact and straight with the presence of spindle-shaped nuclei. The histological tissue sections of the kidney, heart, and liver of Rats treated with FL-ZnO NPs were similar to control samples [Fig. 6 (C)].

4. Discussion

The present study explores the applications of lignin (extracted from plant) and its fragments, FL and its oxidized fragments, OFL, as a template

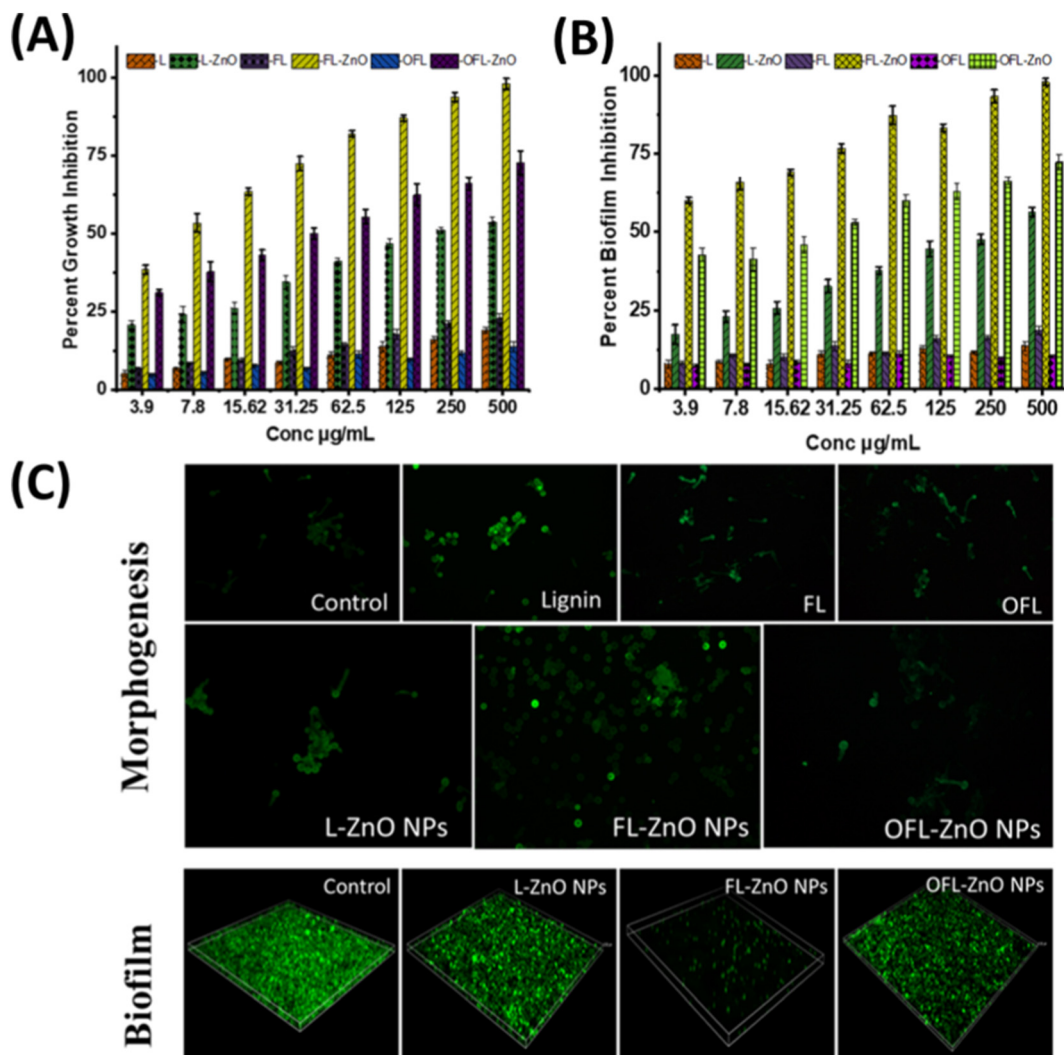


Fig. 4. (A) Percent growth inhibition: Lignin, FL, OFL have not inhibited growth of *C. albicans*. L-ZnO, FL-ZnO and OFL-ZnO NPs inhibited growth to varying extend. Only FL-ZnO has inhibited growth (more than 90%) at 250 µg/mL. (B) Percent biofilm inhibition: Lignin, FL, OFL have not inhibited the biofilm; L-ZnO, FL-ZnO and OFL-ZnO NPs inhibited the biofilm to varying degree. Only FL-ZnO NPs has shown a reduction in biofilm (more than 80%) at 31.25 µg/mL. (C) Morphogenesis: Fluorescence microscopic images of morphogenesis in *C. albicans*. Control, Lignin, FL, OFL, L-ZnO and OFL-ZnO NPs showed morphogenesis (hyphal induction) at 31.2 µg/mL concentrations. However, FL-ZnO NPs inhibited morphogenesis of *C. albicans*. Biofilm: Confocal microscopic images (600 µm scale bar) of biofilm – At 0 µg/mL (control), there was a confluent biofilm, however, at 31.25 µg/mL, the biofilm confluence decreased to 20, 80, and 50%, respectively in presence of L-ZnO, FL-ZnO and OFL-ZnO NPs.

for synthesizing ZnO NPs viz., L-ZnO, FL-ZnO and OFL-ZnO NPs as anti-virulence agents against *C. albicans*. First, we extracted lignin from the bagasse by microwave-assisted methods and partially purified lignin by silica chromatography. The microwave method was used to extract lignin as it extracted a greater quantity of lignin [45]. The partially purified lignin was subjected to fragmentations to form FL, and later FL was oxidized to form OFL. The extracted lignin, FL, and OFL were used for the synthesis of ZnO NPs.

4.1. Characterization of lignin, FL, and OFL

Extracted lignin showed an absorption maximum at 287 nm due to the extended conjugation system of benzene. The OFL showed two peaks, one at 280 nm, which can be accounted for by dimethoxy phenyls of coniferyl alcohol, p-coumaryl alcohol and sinapyl alcohol [46]. Another small peak at 317 nm can be accounted for by the presence of ester or ether linkages [47]. The FL showed an entirely different spectrum. The FL showed an absorption maximum at 424 nm, accounting for $n \rightarrow \pi^*$ transitions. This transition may include conjugated chromophores such as 'O' atom of ester and ether [48]. Different functional groups in the polymer can account for the

broad peak at 1500–1627 cm^{-1} . The prominent peak at 3458 cm^{-1} can be accounted for the presence of the hydroxyl group, or it can be accounted for cellulose impurities [49]. A peak at 1726 cm^{-1} can be accounted to the carbonyl group stretching of an aldehydic group. Peaks at 1500 cm^{-1} and 1627 cm^{-1} can be accounted for the aromatic ring structure in the lignin [50]. The presence of an intense peak at 1726 cm^{-1} can be attributed to CC stretching and were not destroyed in OFL [50]. To identify the FL, we have performed HRMS. The observed m/z can be assigned as follows. The first fragment at 276 m/z may represent 4-(4-(hydroxymethyl)-3-methoxyphenyl)-2-methoxy phenol [51], a second fragment at 290 m/z may represent β -etheral linkage [52], a third fragment at 322 m/z may represent sinapic acid (3-(4-hydroxy-3,5-dimethyl phenyl)prop-2-enoic-acid [53], a fourth fragment at 405 m/z may represent dimeric fragment [54], and the fifth fragment at 534 m/z may represent β -O-4 dimer with an attachment of different carbon atom or $-\text{CH}_2$ group in the molecule [55]. Based on HRMS fragmentation data, fragmentation for lignin may occur, as shown in Fig. 3. Furthermore, we also have performed NMR to gain details of FL and OFL structures. In ^1H NMR, peaks at 0.9–1.5, 3.5–4.2, 4.8–5.8, 6.8–7.48 value correspond to the methylene, aliphatic hydroxyl, and methoxy proton, β -O-4 aryl ether proton, vinylic proton

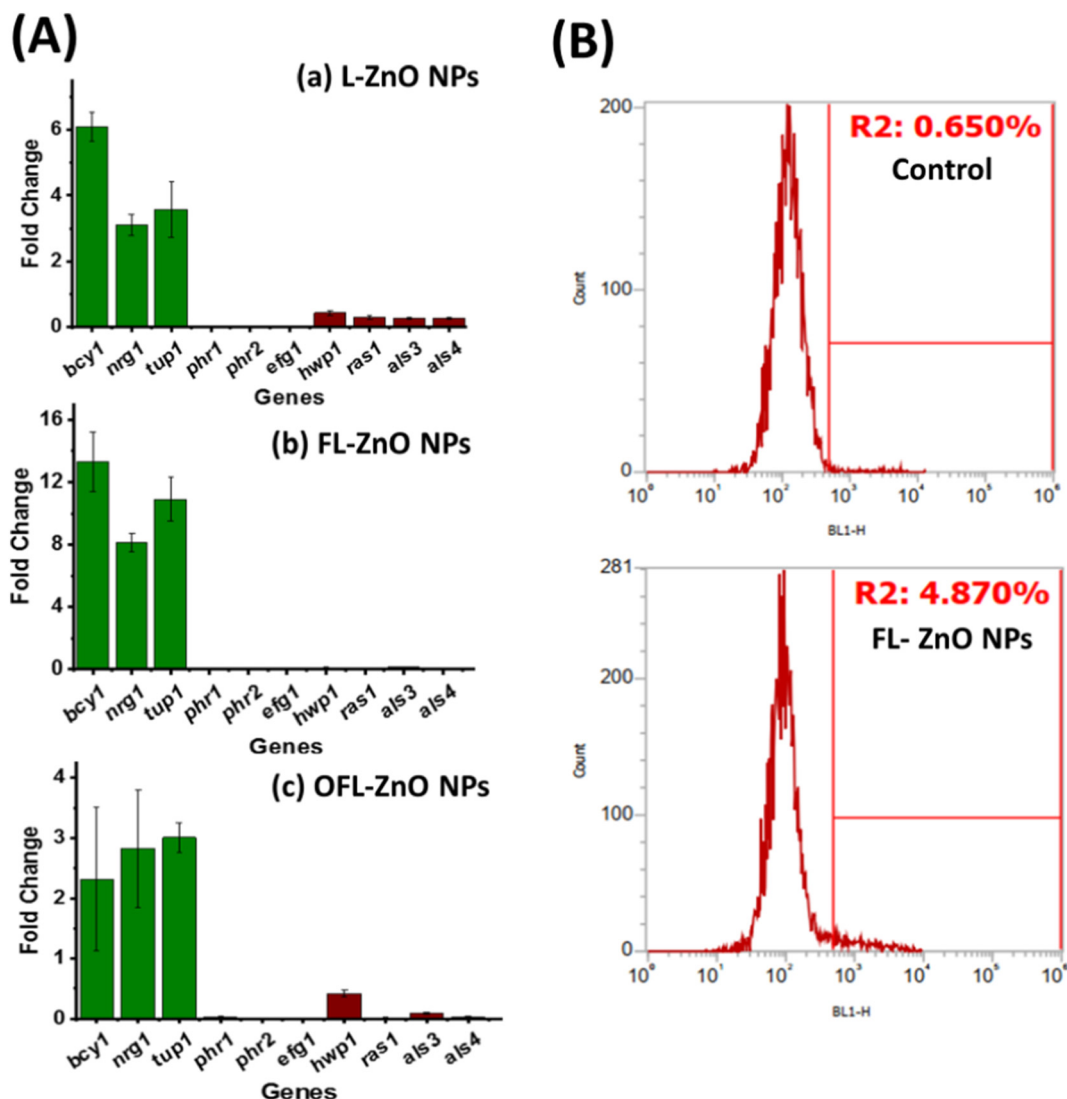


Fig. 5. (A) Gene expression during morphogenesis and biofilm. The genes such as *bcy1*, *nrg1*, and *tup1* were upregulated and genes such as *phr1*, *phr2*, *efg1*, *hwp1*, *ras1*, *als3*, and *als4* were downregulated. The upregulation and downregulation were more prominent in presence of FL-ZnO NPs. (B) ROS determinations: *C. albicans* treated with FL-ZnO NPs (31.25 $\mu\text{g}/\text{mL}$) generated 4.8% ROS in 30 min.

(attached to alkene C), aromatic proton (of p-coumaric acid), respectively. The aromatic proton (6.8–7.4) corresponds to the G-unit, S-unit and H-units conjugated with a double bond or etheral linkage [55]. The weak etheral linkage of lignin breaks down into FL, resulting in the peak broadening for aliphatic hydroxyl proton (3.4–4.2 δ) and methoxy proton (5.8 δ). New peaks at 2.8 and 2.3 δ values were observed for aromatic and aliphatic acetate proton. In OFL, vinylic protons (attached to alkene C) were converted into aldehydic proton at 9.8 δ value, and methylene proton disappeared.

4.2. Synthesis and characterization of L-ZnO, FL-ZnO and OFL-ZnO NPs

After characterization, lignin, FL, and OFL were used for the synthesis of ZnO NPs. A blue shift in the exciton absorption for FL-ZnO NPs indicate the quantum confinement property of FL-ZnO NPs. In the tau plot, an increase in the bandgap was due to the quantum confinement property of ZnO NPs [56]. The major XRD peaks for L-ZnO, FL-ZnO, OFL-ZnO NPs were sharp and intense, indicating the high crystallinity of ZnO NPs. Furthermore, no peaks other than the hexagonal crystalline phase of ZnO NPs were found, indicating the phase purity of the as-synthesized ZnO NPs. The functional groups present on the lignin, FL and OFL played essential roles in the complexing, capping, and stabilization of Zn^{2+} ions and have contributed towards the morphological appearance of ZnO NPs. The L-ZnO NPs showed

spherical agglomerated morphology possible due to the three-dimensional polymeric structure of lignin. The FL promoted simultaneous growth in one dimensional ZnO NPs, resulting in the hierarchical flower-like structure. However, when FL was OFL and used to synthesize ZnO NPs, spherical shaped OFL-ZnO NPs were again formed, possibly due to the conversion of a vinylic group of FL into an aldehydic group. BET is one crucial analysis technique for measuring materials specific surface area and gives the measurement of the surface area of the materials. An increased surface area of FL-ZnO NPs indicates the porous nature of FL-ZnO NPs.

4.3. Effect of L-ZnO, FL-ZnO and OFL-ZnO NPs on the planktonic growth of *C. albicans*

In the present study, we studied two biological applications of ZnO NPs (L-ZnO, FL-ZnO and OFL-ZnO NPs) against *C. albicans*: antimicrobial and anti-virulence. First, we explored the possibility of L-ZnO, FL-ZnO and OFL-ZnO NPs to inhibit the growth of *C. albicans*. The MIC results clearly showed that whereas lignin, FL and OFL were almost inactive, L-ZnO, FL-ZnO and OFL-ZnO NPs inhibited the planktonic growth of *C. albicans*. Recently various nanomaterials were synthesized and tested against *C. albicans*. Chemically and biologically synthesized nanomaterials such as Ag, ZnO, NPs, MgO, Fe_3O_4 , CuO, and Se NPs [24–37,57–58] have been

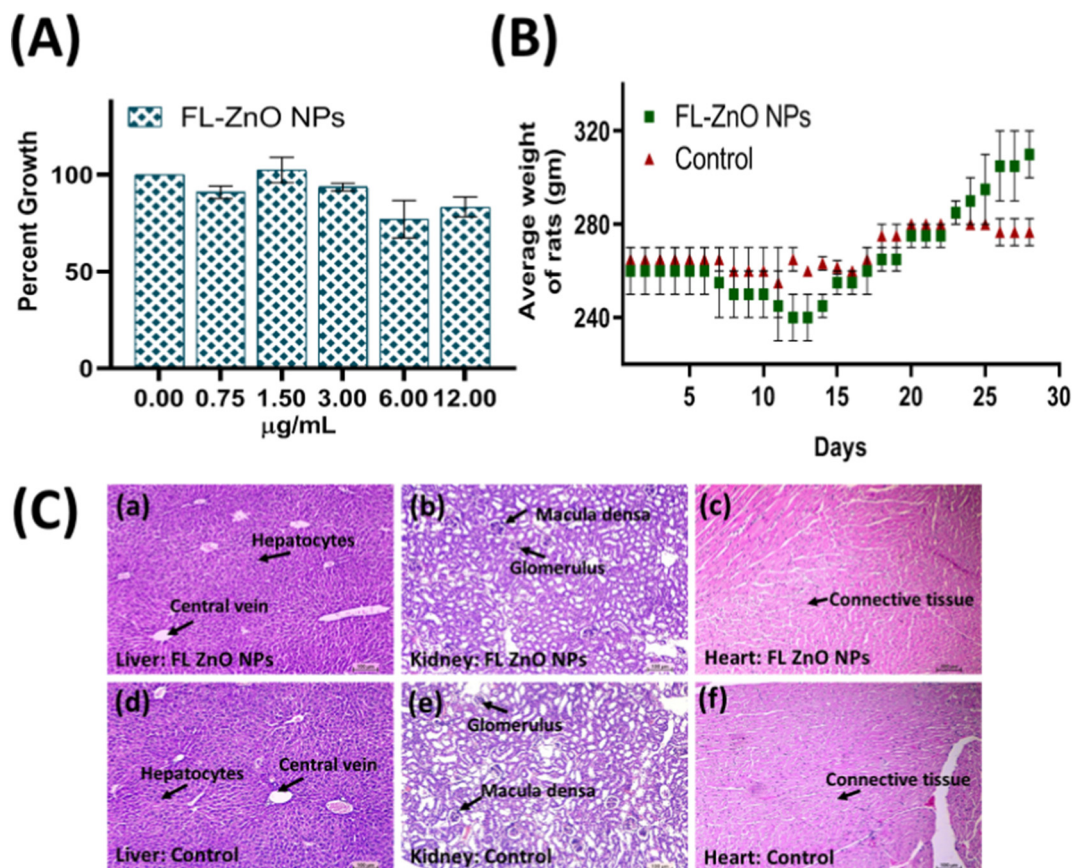


Fig. 6. (A) In-vitro cytotoxicity assay: A 3T3-L1 cell line treated with FL-ZnO NPs showed good cell viability; 80% cells were viable at 12 µg/mL (B) In-vivo animal toxicity study: average change in the weight of Rats for 28 days upon feeding with FL-ZnO NPs. The weight was constant till 12 days, and thereafter increased gradually till 28 days. Rats not fed with FL-ZnO NPs (controls) showed very negligible weight gain. (C) Histological observations of organs: The histopathological examination of liver, kidney and heart tissue after feeding Rats with FL-ZnO NPs. The tissue sections were normal, and no abnormal changes were observed in these organs. In liver section, hepatocytes were normal, in kidney section, macula densa, glomerulus, and basement membrane were intact; in heart section, cardiac muscle cells and connective tissue were intact similar to control (d), (e), and (f) respectively.

shown to inhibit the growth or biofilm of *C. albicans* on various surfaces. In contrast, nanomaterials synthesized using biological methods have the advantage of low cytotoxicity and the ability to functionalize the surfaces with organic molecules. Therefore, in recent times, plant extract, seaweeds, and biomolecules were used to synthesize ZnO NPs against *C. albicans*. The leaf extract of *Glycosmis pentaphylla* was used to synthesize ZnO NPs of 32 to 36 nm and was shown to inhibit the growth of *C. albicans* at the concentration of 100 µg/mL [59]. Similarly, the leaf extract of *Azadirachta indica* was used to synthesize ZnO NPs and was shown to inhibit the growth of *C. albicans* at MIC value of 200 µg/mL [60]. ZnO NPs prepared from leaf extract of *Crinum latifolium* have inhibited the growth and virulence system of *C. albicans* [25]. Interestingly, the MIC of ZnO NPs in some studies were relatively high, 500 µg/mL [26]. Apart from terrestrial plant materials (above reports), sea plants, such as seaweeds viz., green *Caulerpa peltata*, red *Hypnea valencia* and brown *Sargassum myriocystum* were also used to synthesize ZnO NPs. However, only ZnO NPs prepared from *S. myriocystum* could show anti-*Candidal* activity with MIC value of 1000 µg/mL, which is a very high MIC value reported to date [61]. In comparison to the reports mentioned above, the MIC value of FL-ZnO for inhibiting the growth of *C. albicans* in the present study is low, indicating the importance of FL towards the synthesis of anti-*Candidal* ZnO NPs. When we compared the growth inhibition abilities of *C. albicans* with ZnO NPs prepared from or stabilized with macromolecules such as lignin [35], chitosan [57] and chitosan-linoleic acid [32], it appeared that FL-ZnO NPs in the present study showed far better anti-*Candidal* activity against *C. albicans* because the concentrations required to bring about the reduction in the growth of *C. albicans* was lower than the reports above. Recently attempts were

made to find out the mechanism of action of ZnO containing nanomaterials on *Candida*. There have been reports that some nanomaterials act as antioxidants [62,63], while others produce reactive oxygen species (ROS) [64, 65]. Shoeb et al., (2013) [66] has demonstrated that ZnO NPs interact with the cell surfaces of *C. albicans*. ROS generated by such interactions included superoxide (O_2^-) and hydroxyl (OH^\bullet) radicals. These radicals act on membranes, leading to membrane integrity, eventually inhibiting the growth of *C. albicans* [66,67]. However, in our study, the ROS produced was less, and therefore, we rule out the ROS mediated cell membrane damage for the antimicrobial action of FL-ZnO NPs.

Recently, it has been shown that some nanomaterials, such as gold nanoparticles (Au NPs), act on *C. albicans* by ROS-independent mechanism. The Au NPs were shown to act on *C. albicans* by disrupting mitochondrial calcium homeostasis and mitochondrial membrane potential [68]. In the light of the antimicrobial action of Au NPs, in the present study, we report the ROS-independent antifungal mechanism of FL-ZnO NPs on *C. albicans*. It is likely possible that FL-ZnO NPs may damage the DNA or cause mitochondrial dysfunctions, as reported in the case of Au NPs. Nevertheless, further studies are needed to understand FL-ZnO NPs' action on *C. albicans*.

4.4. Morphogenesis inhibition

The virulence attributes of *C. albicans* include morphogenesis (transition from yeast to hypha) and biofilm. The morphogenesis help *C. albicans* to evade mucous membrane and tissues and provide an opportunity to enter the bloodstream, thereby causing greater damage [5]. Therefore, inhibition of morphogenesis is likely to abolish the virulence

attributes of *C. albicans*, thereby assisting the present antifungal therapies. Recently, few nanomaterials such as Ag NPs [30,58], ZnO NPs [25,26], and MgO [32] were shown to inhibit morphogenesis in *C. albicans*. The Ag NPs synthesized using the methanolic leaf extract from *Dodonaea viscosa*, and *Hyptis suaveolens* plants were shown to inhibit morphogenesis and macro-colony formation, probably, at 10 µg/mL [58]. The morphogenesis inhibition was shown to be size-dependent [30], smallest sized NPs inhibited morphogenesis effectively. Similarly, MgO NPs prepared by the hydrothermal method were shown to inhibit morphogenesis in *C. albicans* at a calculated concentration of 297 µg/mL [31]. The ZnO NPs prepared using a biological approach (leaf extract of *C. latifolium*) also were shown to inhibit morphogenesis; however, the concentrations of NPs required to bring out morphogenesis were high, about 1 mg/mL [26].

In the present study, the ZnO NPs synthesized by using FL are promising nanomaterials against *C. albicans* because the amount of FL-ZnO NPs required to inhibit the morphogenesis was significantly less than the reports mentioned above. Notably, the bioactive ZnO NPs, which inhibited morphogenesis in *C. albicans*, were prepared using agro-wastes.

4.5. Biofilm inhibition

As mentioned before, the biofilm of *C. albicans* is a complex network of heterogeneous populations comprising biphasic distribution of yeast and filamentous cells. The sessile cells and hyphal form of *C. albicans* inside the biofilm are highly virulent (>1000 times more resistant to antifungal drugs). Therefore, there is an urgent need for novel approaches to target the biofilm of *C. albicans* as biofilm has an essential role in the pathogenesis of *C. albicans*. Recently, numerous nanomaterials were explored to inhibit or disrupt the biofilm. Nanomaterials like Ag NPs [25,27,29], MgO NPs [31], and ZnO NPs [26,33] were shown to inhibit the biofilm of *C. albicans* to a varying degree depending on the type and size of nanomaterials. Ag NPs with spherical, quasi-spherical and hexagonal shapes and sizes ranging from 1 to 100 nm was shown to decrease biofilm [30]. The biofilm decrease was more prominent in the presence of spherical Ag NPs. Furthermore, the biofilm inhibition efficacy of spherical shaped Ag NPs was dependent on the size of NPs. Ag NPs of 7.0 nm was shown to decrease the biofilm formation most efficiently in comparison to the Ag NPs of size 21.4 and 50.3 nm [30]. The biofilm of *C. albicans* in the presence of MgO NPs [31] and CuO NPs and Cu₂O NPs was also remarkable reduced [57]. Recently, bio-fabricated ZnO NPs were also shown to decrease the biofilm of *C. albicans* effectively. Leaf extract of *P. pinnate* was used to prepare spherical shaped ZnO NPs with an average particle size of 35 nm, which reduced the biofilm to 42% at 50 µg/mL [69]. In another study, *Crinum latifolium* was used to prepare spherical ZnO NPs with a size range of 10–30 nm, reducing biofilm formation at 250 µg/mL, with some cells showing abnormal cells or damaged structures [26]. It is interesting to report that, like previous reports, the present study also reports the synthesis of ZnO NPs using plant (lignin, FL and OFL) materials. However, unlike earlier reports, the present study reports a relatively lesser concentration of FL-ZnO NPs to inhibit the biofilm of *C. albicans*. One of the reasons for such effective biofilm inhibition may be the porous structure of ZnO NPs, which might have increased the surface reactivity of FL-ZnO NPs. Therefore, the inhibition of biofilm in the presence of F-ZnO NPs will make *C. albicans* susceptible to various antibiotics therapies or render *C. albicans* avirulent.

4.6. Gene expression analysis

To understand the molecular mechanisms behind morphogenesis, we analyzed the levels of expressed genes when *C. albicans* were treated with FL-ZnO NPs via RT-PCR study. L-ZnO, FL-ZnO, and OFL-ZnO NPs modulated the molecular mechanisms that upregulated the negative regulators and downregulated the positive regulators of morphogenesis and biofilm. The *bcy1* plays an important role in the cell differentiation and death of *C. albicans*. The deletion of *bcy1* gene leads to the development of filamentous hyphal growth [70]. In other words, up-regulation of *bcy1* gene expression represses filamentous growth. The upregulation of *bcy1* in the presence

of L-ZnO, FL-ZnO, and OFL-ZnO NPs (respectively, 6.0, 13.0, 2.3-fold) essentially repressed the formation of filamentous growth. The *nrg1* gene plays an important role in the negative regulation of morphogenesis. The upregulation of *nrg1* gene represses morphogenesis and represses hypha-specific genes [71]. The upregulation of *nrg1* in the presence of L-ZnO, FL-ZnO, and OFL-ZnO NPs (respectively, 3.0, 8.4, and 2.8-fold) essentially, therefore, repressed the hypha-specific genes. The *tup1* plays an important role in the transition of yeast to hyphae and governs the regulation of genes, including those involved in virulence. The expression of *tup1* represses the expression of genes that are essential for the formation of the hypha. The deletion of *tup1* promotes filamentous growth [72]. The upregulation of *tup1* in the presence of L-ZnO, FL-ZnO, and OFL-ZnO NPs (respectively, 3.5, 10.9, and 3.0-fold) essentially, therefore, repressed the expression of genes necessary for hypha formation. The *hwp1* is among the most well-characterized *C. albicans* gene and is involved in the assemblage of the cell wall, morphogenesis, and promoting attachment of *C. albicans* to epithelial cells [73]. The *hwp1* is upregulated during the formation of the germ tube and downregulated during the yeast form of growth. It is suggested that the cells of *C. albicans* which have the *hwp1* protein, are more virulent and can initiate the infection [74]. The downregulation of *hwp1* in the presence of L-ZnO, FL-ZnO, and OFL-ZnO NPs (respectively, 0.433, 0.107, and 0.419-fold) essentially, therefore, repressed the germ tube formation and hyphal development. The *als* genes promote the adhesion of *C. albicans* to host surfaces and promote biofilm on surfaces [75]. *Als* family of proteins help *C. albicans* for initial binding to epithelial cells, endothelial cells, and extracellular matrix proteins and later help *C. albicans* to invade host cells and obtain iron. The *als3* gene is essential for the successful establishment of *Candida* infection [76,77]. *Als3* protein influences the biofilm formation abilities of *C. albicans* on a variety of substrata, such as polystyrene and silicone elastomer. The downregulation of *als3*, *als4* genes in the presence of L-ZnO, FL-ZnO, and OFL-ZnO NPs essentially de-mediated attachment of *C. albicans* to various biological surfaces abolish the initiation of fungal infection. The *ras1* genes play a pivotal role in the regulation of MAP kinase and a cAMP signaling pathway. By activating these pathways, virulence traits such as yeast-to-filament conversion, biofilm formation, phenotypic switching, and stress resistance can be modulated. Mutants lacking *ras1* are defective in filamentous growth. [78,79]. The downregulation of *ras1* in the presence of L-ZnO, FL-ZnO, and OFL-ZnO NPs (respectively, 0.299, 0.022, and 0.019-fold) essentially, therefore, repressed the modulations of traits required for virulence such as biofilm formation, phenotypic switching, and stress resistance. The *efg1* encodes a transcription factor that regulates morphogenetic regulations in *C. albicans*, such as chlamyospore formation, phenotypic switching, and filamentous growth. The *efg1* plays a crucial role in the expression of cell wall proteins such as *hwp1* or *als*. The *efg1* induces pseudohyphal growth, and overexpression of the *efg1* enhances mycelial growth [80]. The downregulation of *efg1* in the presence of L-ZnO, FL-ZnO, and OFL-ZnO NPs (respectively, 0.018, 0.002, and 0.002-fold) repressed morphogenetic regulations in *C. albicans* such as chlamyospore formation, phenotypic switching, and filamentous growth. The *phr1* and *phr2* expression promotes the adherence of *C. albicans* to epithelial cells and polystyrene and help in the formation of biofilm. Expression of *phr1* increase the polysaccharide synthesis (during biofilm formation) and decreases in the absence of *phr1* genes [81]. The downregulation of *phr1* and *phr2* in the presence of L-ZnO, FL-ZnO, and OFL-ZnO NPs essentially, therefore, repressed the biofilm formation and the adherence of *C. albicans* to epithelial cells and polystyrene. An analysis of differential gene expression during morphogenesis inhibition showed that the upregulation of negative regulators and the downregulation of positive regulators of morphogenesis and biofilm of *C. albicans* were prominently affected by FL-ZnO NPs.

4.7. Biocompatibility study of FL-ZnO NPs in vivo animal model

It has been documented that some nanomaterials create an adverse effect on humans. A recent study showed that Ag NPs reduce selenoprotein synthesis and thioredoxin reductase activity in keratinocytes and lung

cells [82]. Similarly, ZnO NPs were also shown to cause a loss in body weight, passive behavior, and reduced survival of cells [83,84]. Therefore, we decided to study the biocompatibility of FL-ZnO NPs. The FL-ZnO NPs did not reduce the viability of 3T3-L1 to a significant extent, indicating they are not cytotoxic. Similarly, the histological tissue sections of the kidney, heart, and liver had no abnormalities in any of the tissue sections showing that as-synthesized FL-ZnO NPs were not toxic at tested concentrations. We believed that FL would have modified the surface chemical structures, surface charge density, or the catalytic activity of ZnO NPs, and would have made ZnO NPs biocompatibility [85].

5. Conclusion

In the present study, lignin, FL and OFL were successfully used to synthesize L-ZnO, FL-ZnO, and OFL-ZnO NPs. Among all ZnO NPs viz., L-ZnO, FL-ZnO, and OFL-ZnO NPs, FL-ZnO NPs have successfully inhibited the growth, morphogenesis, and biofilm of *C. albicans*. FL-ZnO NPs may act on *C. albicans* by ROS-independent mechanisms, possibly causing DNA damage and mitochondria dysfunction for anti-*Candida* activity, downregulating the positive regulator of morphogenesis and biofilm, and upregulated the negative regulators of morphogenesis and biofilm. The FL-ZnO NPs were noncytotoxic on 3T3-L1 cells and had not shown any histological abnormalities in the liver, heart, and kidney tissue sections. The present study's finding suggested that FL-ZnO NPs could be employed as promising anti-virulence agents to prevent the virulence attributes in *C. albicans* by inhibiting the key virulence factors and biofilms. The present study opens several avenues of further studies related to the design and fabrication of surface materials for inhibiting the growth and virulence system of *C. albicans* on various biotic and abiotic surfaces.

Author statement

All authors acknowledge that the material presented in this manuscript has not been previously published, except in abstract form, nor is it simultaneously under consideration by any other journal.

Ethical statement

The animal studies were done at the Department of Veterinary Pathology, Krantishinh Nana Patil College of Veterinary Science (KNPCVS), Shirval, Dist. Satara. All animal experiments were performed following national guidelines for the care and handling of laboratory animals and following the recommendation in the Guide for the Care and Use of Laboratory animals of the Committee for Control and Supervision on Animals (CPCSEA) in India. (Reference No: SGRS/IAEC/22/2018-19).

Contributions

Kanchan Joshi synthesized and characterized nanoparticles, Amruta Shelar performed experiments on *Candida albicans*, Umesh Kasabe performed characterization of nanoparticles, Latesh Nikam and Bharat Kale supervised nanoparticle synthesis related work, Jaiprakash Sangshetti and Ramdas Pawar supervised lignin extraction and characterizations, Ajay Singh edited the manuscript, Rajendra Patil wrote the manuscript and supervised the biological work, and Manohar Chaskar design the work and supervised animal studies.

Declaration of competing interest

All authors declare that there is no conflict of interest.

Acknowledgements

Dr. Manohar G. Chaskar would like to thank Prof. Ramakrishna More A.S.C College for providing research facilities. Also we thanks for C-MET

Pune and Department of Biotechnology of Savitribai Phule Pune University, Pune. Rajendra Patil acknowledges the support from DST PURSE (2017-2018), UPE-II programme (2017-2018) of SPPU, and Biotechnology Department instrument facilities.

References

- [1] P.L. Fidel, in: G.W. Tannock (Ed.), Medical Importance of the Normal Microflora, Boston, MA, Springer, US 1999, pp. 441–476, <https://doi.org/10.1007/978-1-4757-3021-0-18>.
- [2] M.-C. Dignani, J.S. Solomkin, E.J. Anaissie, Candida, in: E.J. Anaissie, McGinnis MR, M.A. Pfaller (Eds.), Clinical Mycology Edinburgh. Churchill Livingstone, Second Edition 2009, pp. 197–229, CHAPTER 8.
- [3] J.J. Limon, J.H. Skalski, D.M. Underhill, Commensal fungi in health and disease, Cell Host Microbe 9 (2017) 156–165, <https://doi.org/10.1016/j.chom.2017.07.002>.
- [4] I.D. Jacobsen, M.J. Niemiec, M. Kapitan, M. Polke, In, Reference module in life sciences, Elsevier (2020) <https://doi.org/10.1016/B978-0-12-809633-8.21281-8>.
- [5] L.P. Erwig, N.A.R. Gow, Interactions of fungal pathogens with phagocytes, Nat. Rev. Microbiol. 14 (2016) 163–176, <https://doi.org/10.1038/nrmicro.2015.21>.
- [6] J.M. Bain, J. Louw, L.E. Lewis, Candida albicans hypha formation and mannann masking of β -glucan inhibit macrophage phagosome maturation, MBio 5 (2014) <https://doi.org/10.1128/mBio.01874-14>.
- [7] J. Chandra, D.M. Kuhn, P.K. Mukherjee, L.L. Hoyer, T. McCormick, M.A. Ghannoum, Biofilm formation by the fungal pathogen Candida albicans: development architecture and drug resistance, J. Bacteriol. 183 (2001) 5385–5394, <https://doi.org/10.1128/jb.183.18.5385-5394.2001>.
- [8] M. Gulati, C.J. Nobile, Candida albicans biofilms: development, regulation, and molecular mechanisms, Microbes Infect. 18 (2016) <https://doi.org/10.1016/j.micinf.2016.01.002>.
- [9] H.-C. Flemming, J. Wingender, The biofilm matrix, nature review, Microbiology 8 (2010) 623–633, <https://doi.org/10.1038/nrmicro2415>.
- [10] J.F. Kernien, B.D. Snarr, D.C. Sheppard, J.E. Nett, The Interface between fungal biofilms and innate immunity, Front. Immunol. 8 (2018) 1968, <https://doi.org/10.3389/fimmu.2017.01968>.
- [11] M.B. Marak, B. Dhanashree, Antifungal susceptibility and biofilm production of Candida spp. isolated from clinical samples, Int. J. Microbiol. (2018), 7495218 <https://doi.org/10.1155/2018/7495218>.
- [12] H.T. Taff, K.F. Mitchell, J.A. Edward, D.R. Andes, Mechanisms of Candida biofilm drug resistance, Future Microbiol. 8 (2013) 1325–1337, <https://doi.org/10.1022/fmb.13.13.101>.
- [13] C.J. Nobile, A.D. Johnson, Candida albicans biofilms and human disease, Annu. Rev. Microbiol. 69 (2015) 71–92, <https://doi.org/10.1146/annurev-micro-091014-104330>.
- [14] M.S. Ahmad Khan, F. Alshehrei, S.B. Al-Ghamdi, M.A. Bamaga, A.S. Al-Thubiani, M.Z. Alam, Virulence and biofilms as promising targets in developing antipathogenic drugs against candidiasis, Future Science 6 (2020), FSO440 <https://doi.org/10.2144/fsoa-2019-0027> OA.
- [15] O.Fleitas Martínez, M.H. Cardoso, S.M. Ribeiro, O.L. Franco, Recent advances in antivirulence therapeutic strategies with a focus on dismantling bacterial membrane micro domains toxin neutralization quorum-sensing interference and biofilm inhibition, Frontiers in Cellular and Infection Microbiology 9 (2019) 74, <https://doi.org/10.3389/fcimb.2019.00074>.
- [16] M. Spitzer, N. Robbins, G.D. Wright, Combinatorial strategies for combating invasive fungal infections, Virulence 8 (2017) 169–185, <https://doi.org/10.1080/21505594.2016.1196300>.
- [17] Q. Liu, A. Zhang, R. Wang, Q. Zhang, D. Cui, A review on metal- and metal oxide-based nanozymes: properties, mechanisms, and applications, Nano-Micro Lett. 13 (1) (2021) 154, <https://doi.org/10.1007/s40820-021-00674-8>.
- [18] L. Mei, S. Zhu, Y. Liu, W. Yin, Z. Gu, Y. Zhao, An overview of the use of nanozymes in antibacterial applications, Chem. Eng. J. 418 (2021), 129431 <https://doi.org/10.1016/j.cej.2021.129431>.
- [19] N.V.S. Vallabani, A. Vinu, S. Singh, A. Karakoti, Tuning the ATP-triggered pro-oxidant activity of iron oxide-based nanozyme towards an efficient antibacterial strategy, J. Colloid Interface Sci. 567 (2020) 154–164, <https://doi.org/10.1016/j.jcis.2020.01.099>.
- [20] I.E. Mba, E.I. Nweze, The use of nanoparticles as alternative therapeutic agents against Candida infections: an up-to-date overview and future perspectives, World Journal of Microbiology and Biotechnology 36 (11) (2020) 163.
- [21] A.V. Singh, M. Ferri, M. Tamplenizza, Bottom-up engineering of the surface roughness of nanostructured cubic zirconia to control cell adhesion, Nanotechnology 23 (2012), 475101 <https://doi.org/10.1088/0957-4484/23/47/475101>.
- [22] A.V. Singh, V. Vyas, R. Patil, Quantitative characterization of the influence of the nano-scale morphology of nanostructured surfaces on bacterial adhesion and biofilm formation, PLOS ONE 6 (9) (2011), e25029 <https://doi.org/10.1371/journal.pone.0025029>.
- [23] P.P. Mahamuni-Badiger, P.M. Patil, M.V. Badiger, P.R. Patel, B.S. Thorat-Gadgil, A. Pandit, R.A. Bohara, Biofilm formation to inhibition: role of zinc oxide-based nanoparticles, 108 (2020), 110319 <https://doi.org/10.1016/j.jmse.2019.110319>.
- [24] M. Jalal, A.M. Ansari, M.A. Alzohairy, S.G. Ali, H.M. Khan, A. Almatroudi, M.I. Siddiqui, Anti-Candidal activity of biosynthesized silver nanoparticles: effect on growth cell morphology and key virulence attributes of Candida species, Int. J. Nanomedicine 14 (2019) 4667–4679, <https://doi.org/10.2147/ijn.S210449>.
- [25] M. Jalal, M.A. Ansari, S.G. Ali, H.M. Khan, S. Rehman, Anti-Candidal activity of bio inspired ZnO NPs: effect on growth cell morphology and key virulence attributes of Candida species, Artif. Cells Nanomed. Biotechnol. 46 (2018) 912–925, <https://doi.org/10.1080/21691401.2018.1439837>.
- [26] H.H. Lara, D.G. Romero-Urbina, C. Pierce, J.L. Lopez-Ribot, Effect of silver nanoparticles on Candida albicans biofilms an ultra-structural study, J. Nanobiotechnol. 13 (2015) <https://doi.org/10.1186/s12951-015-0147-8>.

- [27] M.S. Al Aboody, Silver/silver chloride (Ag/AgCl) nanoparticles synthesized from *Azadirachta indica* latex and its antibiofilm activity against fluconazole resistant *Candida tropicalis*, *Artif. Cells Nanomed. Biotechnol.* 47 (2019) 2107–2113, <https://doi.org/10.1080/21691401.2019.1620257>.
- [28] D.R. Monteiro, L.F. Gorup, S. Silva, M. Negri, E.R. de Camargo, R. Oliveira, D.B. Barbosa, M. Henriques, Silver colloidal nanoparticles: antifungal effect against adhered cells and biofilms of *Candida albicans* and *Candida glabrata*, *Biofouling* 27 (2011) 711–719, <https://doi.org/10.1080/08927014.2011.599101>.
- [29] B. Szerencsés, N. Igaz, Á. Tóbiás, Z. Pruci, A. Rónavári, P. Béteky, D. Madarász, C. Papp, I. Makra, C. Vágvölgyi, Z. Kónya, I. Pfeiffer, M. Kirics, *BMC Microbiol.* 20 (2020) 176, <https://doi.org/10.1186/s12866-020-01858-9>.
- [30] F. Kong, R. Han, J. Yue, Antifungal activity of magnesium oxide nanoparticles: effect on the growth and key virulence factors of *Candida albicans*, *Mycopathologia* 185 (2020) 485–494, <https://doi.org/10.1007/s11046-020-00446-9>.
- [31] S. Barad, M. Roudbary, A.N. Omran, M.P. Daryasari, Preparation and characterization of ZnO nanoparticles coated by chitosan-linoleic acid; fungal growth and biofilm assay, *Bratisl. Lek. Listy* 118 (2017) 169–174, https://doi.org/10.4149/bl_2017_034.
- [32] S.S. Hosseini, E. Ghaemi, A. Noroozi, F. Niknejad, Zinc oxide nanoparticles inhibition of initial adhesion and ALS1 and ALS3 gene expression in *Candida albicans* strains from urinary tract infections, *Mycopathologia* 184 (2019) 261–271, <https://doi.org/10.1007/s11046-019-00327-w>.
- [33] S.S. Hosseini, H. Jashaghani, T. Shokohi, A. Ahmadi, Z. Mehrbakhsh, Antifungal activity of ZnO nanoparticles and nystatin and downregulation of SAP1-3 genes expression in fluconazole-resistant *Candida albicans* isolates from Vulvovaginal Candidiasis, *Infect. Drug Resist.* 13 (2020) 385–394, <https://doi.org/10.2147/IDR.S226154>.
- [34] L.M. Jose, S. Kuriaakose, S. Thomas, Fabrication, characterization and in vitro antifungal property evaluation of biocompatible lignin-stabilized zinc oxide nanoparticles against selected pathogenic fungal strains, *BioNanoScience* 10 (2020) 583–596, <https://doi.org/10.1007/s12668-020-00748-8>.
- [35] E.M. Ali, B.M. Abdallah, Effective inhibition of Candidiasis using an eco-friendly leaf extract of *calotropis gigantea* mediated silver nanoparticles, *Nanomaterials* 10 (2020) <https://doi.org/10.3390/nano10030422>.
- [36] G. Guisbiers, H.H. Lara, R. Mendoza-Cruz, G. Naranjo, B.A. Vincent, X.G. Peralta, K.L. Nash, Inhibition of *Candida albicans* biofilm by pure selenium nanoparticles synthesized by pulsed laser ablation in liquids, *Nanomed. Nanotechnol. Biol. Med.* 13 (3) (2017) 1095–1103, <https://doi.org/10.1016/j.nano.2016.10.011>.
- [37] A.R. Padmavathi, P.S. Murthy, A. Das, Impediment to growth and yeast-to-hyphae transition in *Candida albicans* by copper oxide nanoparticles, *Biofouling* 36 (2020) 56–72, <https://doi.org/10.1080/08927014.2020.1715371>.
- [38] L.S. Arias, J.P. Pessan, F.N. de Souza Neto, B.H.R. Lima, E.R. de Camargo, G. Ramage, A.C.B. Delbem, D.R. Monteiro, Novel nanocarrier of miconazole based on chitosan-coated iron oxide nanoparticles as a nanotherapy to fight *Candida* biofilms, *Colloids Surf. B: Biointerfaces* 192 (2020), 111080 <https://doi.org/10.1016/j.colsurfb.2020.111080>.
- [39] A. Henn, M.-L. Mattinen, Chemo-enzymatically prepared lignin nanoparticles for value-added applications, *World J. Microbiol. Biotechnol.* 35 (2019) <https://doi.org/10.1007/s11274-019-2697-7>.
- [40] P. Basnet, T. Inakhunbi Chanu, D. Samanta, S. Chatterjee, A review on bio-synthesized zinc oxide nanoparticles using plant extracts as reductants and stabilizing agents, *J. Photochem. Photobiol. B Biol.* 183 (2018) 201–221, <https://doi.org/10.1016/j.jphotobiol.2018.04.036>.
- [41] K.M. Joshi, D.R. Shinde, L.K. Nikam, Fragmented lignin-assisted synthesis of a hierarchical ZnO nanostructure for ammonia gas sensing, *RSC Adv.* 9 (2019) 2484–2492, <https://doi.org/10.1039/C9RA05874A>.
- [42] M.A. Pfaller, C. Grant, V. Morthland, J. Rhine-Chalberg, Comparative evaluation of alternative methods for broth dilution susceptibility testing of fluconazole against *Candida albicans*, *J. Clin. Microbiol.* 32 (1994) 506–509, <https://doi.org/10.1128/jcm.32.2.506-509.1994>.
- [43] J.S. Raut, R.B. Shinde, N.M. Chauhan, S.Mohan Karuppaiyil, Terpenoids of plant origin inhibit morphogenesis, adhesion, and biofilm formation by *Candida albicans*, *Biofouling* 29 (2013) 87–96, <https://doi.org/10.1080/08927014.2012.749398>.
- [44] A.K. Jadhav, P. Jangid, R. Patil, W. Gade, K. Kharat, S.M. Karuppaiyil, Phenazine methosulphate modulating the expression of genes involved in yeast to hyphal form signal transduction in *Candida albicans*, *Advances in Microbiology* 7 (11) (2017) 707, <https://doi.org/10.4236/aim.2017.711056>.
- [45] W. Yunpu, D.A.I. Leilei, F.A.N. Liangliang, S. Shaoqi, L.L.U. Yuhuan, R. Roger, Review of microwave-assisted lignin conversion for renewable fuels and chemicals, *J. Anal. Appl. Pyrolysis* 119 (2016) 104–113, <https://doi.org/10.1016/j.jaap.2016.03.011>.
- [46] O. Lanzalunga, M. Bietti, Photo- and radiation chemical induced degradation of lignin model compounds, *J. Photochem. Photobiol. B Biol.* 56 (2000) 85–108, <https://doi.org/10.1016/S1011-1344>.
- [47] F. Jahan, V. Kumar, G. Rawat, R.K. Saxena, Production of microbial cellulose by a bacterium isolated from fruit, *Appl. Biochem. Biotechnol.* 167 (2012) 1157–1171, <https://doi.org/10.1007/s12010-012-9595-x>.
- [48] Y. Lu, Y.-C. Lu, H.-Q. Hu, F.-J. Xie, X.-Y. Wei, X. Fan, Structural characterization of lignin and its degradation products with spectroscopic methods, *J. Spectrosc.* (2017), 8951658 <https://doi.org/10.1155/2017/8951658>.
- [49] C. Anyika, N.A.M. Asri, Z.A. Majid, A. Yahya, J. Jaafar, Synthesis and characterization of magnetic activated carbon developed from palm kernel shells, *Nanotechnol. Environ. Eng.* 12 (2017) <https://doi.org/10.1007/s41204-017-0027-6>.
- [50] I. Kubovský, D. Kačíková, Structural changes of oak wood main components caused by thermal modification, *Polymer* 12 (2020) <https://doi.org/10.3390/polym12020485>.
- [51] C.G. Boeriu, D. Bravo, R.J.A. Gosselein, J.E.G. Van Dam, Characterization of structure-dependent functional properties of lignin with infrared spectroscopy, *Ind. Crop. Prod.* 20 (2004) 205–218, <https://doi.org/10.1016/j.indcrop.2004.04.022>.
- [52] K. Morreel, O. Dima, H. Kim, Mass spectrometry-based sequencing of lignin oligomers, *Plant Physiol.* 153 (2010) 1464–1478, <https://doi.org/10.1104/pp.110.156489>.
- [53] M. Tien, T.K. Kirk, Lignin-degrading enzyme from *Phanerochaete chrysosporium* purification characterization and catalytic properties of a unique H2O2-requiring oxygenase, *Proc. Natl. Acad. Sci. U.S.A.* 81 (1984) 2280–2284, <https://doi.org/10.1073/pnas.81.8.2280>.
- [54] A. Richel, C. Vanderghem, M. Simon, B. Wathelet, M. Paquot, Evaluation of matrix-assisted laser desorption/ionization mass spectrometry for second-generation lignin, *Anal. Anal. Chem. Insights* 7 (2012) 79–89, <https://doi.org/10.4137/ACI.S10799>.
- [55] X. Zhao, Z. Huang, Y. Zhang, Efficient solid-phase synthesis of acetylated lignin and a comparison of the properties of different modified lignin, *J. Appl. Polym. Sci.* 134 (2017) <https://doi.org/10.1002/app.44276>.
- [56] S. Jagpreet, K. Sukhmeen, K. Gaganpreet, B. Soumen, R. Mohit, Biogenic ZnO nanoparticles: a study of blue shift of optical band gap and photocatalytic degradation of reactive yellow 186 dye under direct sunlight, *Green ProcessSynth.* 8 (2019) 272–280, <https://doi.org/10.1515/gps-2018-0084>.
- [57] S. Dananjaya, R.S. Kumar, M. Yang, C. Nikapitiya, J. Lee, M. De Zoysa, Synthesis, characterization of ZnO-chitosan nanocomposites and evaluation of its antifungal activity against pathogenic *Candida albicans*, *Int. J. Biol. Macromol.* 108 (2018) 1281–1288, <https://doi.org/10.1016/j.ijbiomac.2017.11.046>.
- [58] S. Muthamil, V.A. Devi, B. Balasubramaniam, K. Balamurugan, S.K. Pandian, Green synthesized silver nanoparticles demonstrating enhanced in vitro and in vivo antibiofilm activity against *Candida* spp, *J. Basic Microbiol.* 58 (4) (2018) 343–357, <https://doi.org/10.1002/jobm.201700529>.
- [59] S. Vijayakumar, C. Krishnakumar, P. Arulmozhi, S. Mahadevan, N. Parameswari, Bio-synthesis, characterization and antimicrobial activities of zinc oxide nanoparticles from leaf extract of *Glycosmis pentaphylla* (Retz.) DC, *Microb. Pathog.* 116 (2018) 44–48, <https://doi.org/10.1016/j.micpath.2018.01.003>.
- [60] K. Elumalai, S. Velmurugan, Green synthesis, characterization and antimicrobial activities of zinc oxide nanoparticles from the leaf extract of *Azadirachta indica* (L), *Appl. Surf. Sci.* 345 (2015) 329–336, <https://doi.org/10.1016/j.apsusc.2015.03.176>.
- [61] S. Nagarajan, K.Arumugam Kuppusamy, Extracellular synthesis of zinc oxide nanoparticle using seaweeds of gulf of Mannar India, *J. Nanobiotechnol.* 11 (2013) 39, <https://doi.org/10.1186/1477-3155-11-39>.
- [62] R. Singh, A.S. Karakoti, W. Self, S. Seal, S. Singh, Redox-sensitive cerium oxide nanoparticles protect human keratinocytes from oxidative stress induced by glutathione depletion, *Langmuir* 32 (46) (2016) 12202–12211, <https://doi.org/10.1021/acs.langmuir.6b03022>.
- [63] A. Karakoti, S. Singh, J.M. Dowding, S. Seal, W.T. Self, Redox-active radical scavenging nanomaterials, *Chem. Soc. Rev.* 39 (11) (2010) 4422–4432, <https://doi.org/10.1039/b919677n>.
- [64] M.A. Ansari, A. Baykal, S. Asiri, S. Rehman, Synthesis and characterization of antibacterial activity of spinel chromium-substituted copper ferrite nanoparticles for biomedical application, *J. Inorg. Organomet. Polym. Mater.* 28 (2018) 2316–2327, <https://doi.org/10.1007/s10904-018-0889-5>.
- [65] S. Rehman, S.M. Asiri, F.A. Khan, B.R. Jermy, H. Khan, S. Akhtar, R.A. Jindan, K.M. Khan, A. Qurashi, Biocompatible tin oxide nanoparticles synthesis antibacterial anti-Candidal and cytotoxic activities, *Chem. Sel.* 4 (2019) <https://doi.org/10.1002/slct.201803550>.
- [66] M. Shueb, B.R. Singh, J.A. Khan, W. Khan, B.N. Singh, H.B. Singh, A.H. Naqvi, ROS-dependent anti-Candidal activity of zinc oxide nanoparticles synthesized by using egg albumen as a biotemplate, *Adv. Nat. Sci. Nanosci. Nanotechnol.* 4 (3) (2013), 035015 <https://doi.org/10.1088/2043-6262/4/3/035015>.
- [67] V. Lakshmi Prasanna, R. Vijayaraghavan, Insight into the mechanism of antibacterial activity of ZnO: surface defects mediated reactive oxygen species even in the dark, *Langmuir* 31 (2015) 9155–9162, <https://doi.org/10.1021/acs.langmuir.5b02266>.
- [68] M. Seong, D.G. Lee, Reactive oxygen species-independent apoptotic pathway by gold nanoparticles in *Candida albicans*, *Microbiol. Res.* 207 (2018) 33–40, <https://doi.org/10.1016/j.micres.2017.11.003>.
- [69] B. Malaikozhundan, B. Vaseeharan, S. Vijayakumar, Biological therapeutics of *Pongamia pinnata* coated zinc oxide nanoparticles against clinically important pathogenic bacteria, fungi and MCF-7 breast cancer cells, *Microb. Pathog.* 104 (2017) 268–277, <https://doi.org/10.1016/j.micpath.2017.01.029>.
- [70] X. Ding, C. Cao, Q. Zheng, G. Huang, The regulatory subunit of protein kinase A (Bcy1) in *Candida albicans* plays critical roles in filamentation and white-opaque switching but is not essential for cell growth, *Front. Microbiol.* 7 (2017) 2127, <https://doi.org/10.3389/fmicb.2016.02127>.
- [71] A.M. Murad, P. Leng, M. Straffon, NRG1 represses yeast-hypha morphogenesis and hypha-specific gene expression in *Candida albicans*, *EMBO J.* 20 (2001) 4742–4752, <https://doi.org/10.1093/emboj/20.17.4742>.
- [72] R. Zhao, S.R. Lockhart, K. Daniels, D.R. Soll, Roles of TUP1 in switching, phase maintenance, and phase-specific gene expression in *Candida albicans*, *Eukaryot. Cell* 1 (2002) 353–365, <https://doi.org/10.1128/EC.1.3.353-365.2002>.
- [73] W.L. Chaffin, *Candida albicans* cell wall proteins, *Microbiol. Mol. Biol. Rev.* 72 (2008) 495–544, <https://doi.org/10.1128/MMBR.00032-07>.
- [74] F. Navarro-García, M. Sánchez, C. Nombela, J. Pla, Virulence genes in the pathogenic yeast *Candida albicans*, *FEMS Microbiol. Rev.* 25 (2001) 245–268, <https://doi.org/10.1111/j.1574-6976.2001.tb00577.x>.
- [75] L.L. Hoyer, E. Cota, *Candida albicans* agglutinin-like sequence (Als) family vignettes: a review of Als protein structure and function, *Front. Microbiol.* 7 (2016) <https://doi.org/10.3389/fmicb.2016.00280>.
- [76] Y. Liu, S.G. Filler, *Candida albicans* Als3 a multifunctional adhesin and invasive, *Eukaryot. Cell* 10 (2011) 168–173, <https://doi.org/10.1128/EC.00279-10>.
- [77] L.L. Hoyer, The ALS gene family of *Candida albicans*, *Trends Microbiol.* 9 (2001) 176–180, <https://doi.org/10.1016/s0966-842x>.

- [78] M. Galocha, P. Pais, M. Cavaleiro, D. Pereira, R. Viana, Divergent approaches to virulence in *C. albicans* and *C. glabrata*: two sides of the same coin, *Int. J. Mol. Sci.* 20 (2019) <https://doi.org/10.3390/ijms20092345>.
- [79] D.O. Inglis, G. Sherlock, Ras signaling gets fine-tuned: regulation of multiple pathogenic traits of *Candida albicans*, *Eukaryot. Cell* 12 (2013) 1316–1325, <https://doi.org/10.1128/EC.00094-13>.
- [80] C.S. Noffz, V. Liedschulte Lengeler, J.F. Ernst, Functional mapping of the *Candida albicans* Efg1 regulator, *Eukaryot. Cell* 7 (2008) 881–893, <https://doi.org/10.1128/EC.00033-08>.
- [81] L. Popolo, G. Degani Camilloni, W.A. Fonzi, The PHR family: the role of extracellular transglycosylases in shaping *Candida albicans* cells, *J. Fungi* 3 (2017) <https://doi.org/10.3390/jof3040059>.
- [82] M. Srivastava, S. Singh, W.T. Self, Exposure to Silver Nanoparticles Inhibits Selenoprotein Synthesis and the Activity of Thioredoxin Reductase, 120, 2012, pp. 56–61, <https://doi.org/10.1289/ehp.1103928>, 1.
- [83] R. Patil, I. Das, R.K. Mehta, R. Sahu, A. Sonawane, Zinc-oxide nanoparticles exhibit genotoxic, clastogenic, cytotoxic and actin depolymerization effects by inducing oxidative stress responses in macrophages and adult mice, *Toxicol. Sci.* 150 (2016) 454–472, <https://doi.org/10.1093/toxsci/kfw010>.
- [84] A.V. Singh, P. Laux, A. Luch, Review of emerging concepts in nanotoxicology: opportunities and challenges for safer nanomaterial design, *Toxicol. Mech. Methods* 29 (2019) 378–387, <https://doi.org/10.1080/15376516.2019.1566425>.
- [85] A. Punnoose, K. Dodge, J.W. Rasmussen, J. Chess, D. Wingett, C. Anders, Cytotoxicity of ZnO nanoparticles can be tailored by modifying their surface structure: a green chemistry approach for safer nanomaterials, *Sustain. Chem. Eng.* 2 (2014) 1666–1673, <https://doi.org/10.1021/sc500140x>.

